A New Method to Detection of Laser Focal Position based on Microlens Array

Duc Duong Nguyen

School of Mechanical Engineering, Hanoi University of Science and Technology, 1 Dai Co Viet, 100000 Hanoi, Vietnam
Institute of Science and Technology, Ministry of Public Security, 47 Pham Van Dong, 100000 Hanoi, Vietnam

Vu Yen Nhi Thai, Dang Khoa Tao, Thi Phuong Anh Nguyen

School of Mechanical Engineering, Hanoi University of Science and Technology, 1 Dai Co Viet, 100000 Hanoi, Vietnam
nhi.tvy195804@sis.hust.edu.vn; anh.ntp222170M@sis.hust.edu.vn

Xuan Binh Cao, Cuc Nguyen Thi Kim

Precision Engineering & Smart measurements Lab, School of Mechanical Engineering, Hanoi University of Science and Technology,
1 Dai Co Viet, 100000 Hanoi, Vietnam
binh.caoxuan@hust.edu.vn; cuc.nguyethikim@hust.edu.vn

Abstract: Many practical uses have been proven by purposely controlling light propagation to achieve adequate non-contact effects on materials. Delivering high-power light into a small region on the materials' surfaces, known as light focusing, allows us to perform several processing methods, such as laser ablation, treatment, or scanning. One of the major goals in laser focusing includes the ability of the system to attain fast and precise focusing on the target surface. To enhance the precision and efficiency of focal point detection in laser processing, a simulation study of laser beam focusing with the use of microlens array is presented. The effects of the microlens array on laser beam focusing are examined by applying the theoretical theory to the simulated optical system in OpticStudio. Our findings show that microlens array-based laser beam focusing increases laser system performance significantly with a simulated result of up to 8% different from the theoretical calculations, and that simulation modeling can be a valuable tool for refining optical models in laser focusing.

Keywords: focal point detection; laser focus; microlens array

1 Introduction

The field of opto-mechanical engineering has gained significant interest in developing autofocus mechanisms. However, there is currently no research on auto-focusing systems that make use of the optical component's features. In the field of laser machining technology, achieving accurate focus is critical for excellent precision throughout the machining process. Microlens array is a versatile technology with various applications. It is used for laser beam shaping, communication, sensor integration, and wavefront sensing, such as Shack-Hartmann measurement. It can also be used to improve image quality by reducing chromatic aberration and increasing the field of view, i.e., in 3D imaging, to enhance the efficiency of light-emitting devices like OLEDs or solar cells [1]. Microlens array has gained more attention for its potential use in measuring radii of aspherical surfaces [2] and in scanning systems [3]. Nonetheless, there is currently no study in auto-focusing systems that utilize these properties of the optical component.

Several auto-focusing methods for laser manufacturing have been developed over the past two decades. Numerous autofocus techniques have been developed; however, they frequently struggle with the balance between accuracy and efficiency. In laser machining technology, the focal point represents the precise location on the cutting surface where the laser beam achieves minimal width and maximum energy level. This ensures the highest level of precision during the machining process. When employed in an arbitrary laser machining system, a focus-finding method is evaluated based on the accuracy and speed of detecting the focal point. Several proposed solutions address the autofocus challenge by leveraging various types of signals generated during the machining process, such as optical signals [4]-[7], [8] or acoustic signals [9], [10]. These methods have found application across a range of machining and measurement fields using laser beams [11]-[15], particularly in critical domains like circuit fabrication, drilling, cutting, and nanostructure inspection. The increasing interest in achieving autofocus has led to the development of advanced automatic focal systems through extensive research. These systems enable precise and efficient laser machining in various industrial applications by optimizing the detection methods and using different signal types. However, the common issue with the methods mentioned above is the dilemma of accuracy and efficiency. A simple-setup system usually takes less time to conduct results but has lower accuracy, such as in the suggested system of Cao et al. [11]-[13]. More precise systems often require complex setups or take longer to detect the focal point, for instance, the proposed method of Chen et al. [14], [15]. In this system, a microlens array is involved to find the focal position. As the microlens array is the only optical component utilized for image capturing on the CCD camera, the aberrations can of the system is trivial and can be actively canceled by calculations. Each lenslet has a considerably small size, therefore, the system is also very sensitive to any changes on the target surface.

This study provides the theoretical model and calculations needed to conduct the method. Next, we perform experiments on OpticStudio to collect data and verify the theoretical model. We then compare the results with previous calculations and discuss the results.

2 Theoretical Analysis

This section presents the schematic diagram of an optical system designed to detect deviations from the focal point position F_1 and the processed surface S. The laser beam from laser source (LS) passes through the beam splitter (BS) and lens L_1 to converge onto the workpiece surface. At the surface, which is considered as a reflective flat mirror, the laser beam is reflected through L_1, reflected at BS, and then reaches L_2, ultimately forming a pattern of spots on the image sensor (IS) (see Figure 1). The optical system is initially adjusted so that the laser beam remains parallel upon reaching L_2, forming a matrix of focal points on IS (i.e. surface S is coincided with F_1 and IS is placed at the focal plane of L_2). Based on the variations in the position of the spots on IS, the deviation from the focal point of S can be calculated. The variations of the spots include sample surface defocus and optical aberration therefore we have two problems:

(1) Find relation between surface defocus and spots variation

(2) Impact of optical aberration to location of the spots

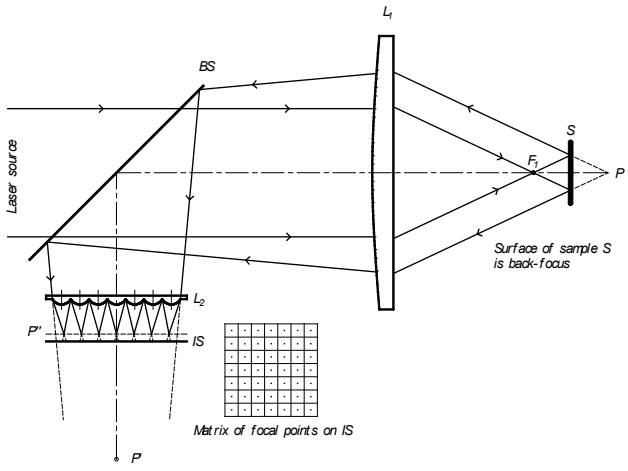

Figure 1
Schematic of the proposed focus detection system with microlens array configuration

For convenience in later calculations, Figure 2 demonstrates the working principle of the proposed system. The schematic uses several mathematical notations, as presented below:

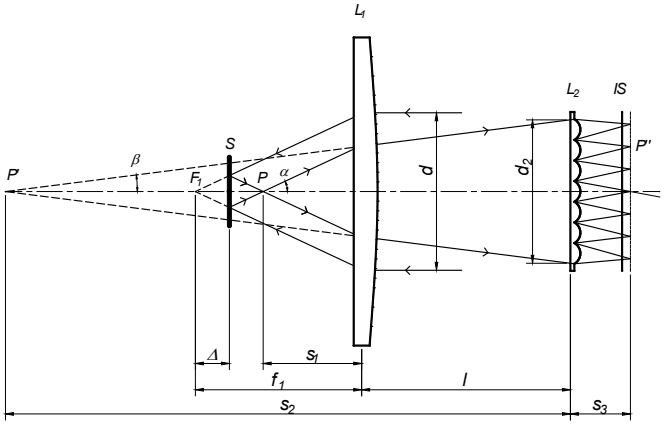

Figure 2
Working principle of the optical system

Surface S is considered a perfect reflector; therefore, we have $PS = F_1S$. The distance from point P (see Figure 2) to lens L_1 is s_1, can be calculated as:

$$s_1 = 2\Delta - f_1 \tag{1}$$

According to the sign convention, the focal length of a converging lens L_1 is positive ($f_1 > 0$) while the distance s_1 is to the left so $s_1 < 0$, the angle α above the optical axis is counterclockwise so $\alpha > 0$.

$$\tan\alpha = \frac{d}{2f_1} \tag{2}$$

Here, f_1 is the focal length of lens L_1, and Δ is the defocus range from S (Δ = 0 in-focus, Δ < 0 back-focus, Δ > 0 front-focus).

Apply the Gauss [16] formula for lens L_1

$$\frac{1}{l+s_2} = \frac{1}{s_1} + \frac{1}{f_1} \Leftrightarrow s_2 = \frac{s_1 f_1}{s_1 + f_1} - l \tag{3}$$

with s_2 is the distance from point *P'* to lens L_2, *l* is the total distance from L_1 to L_2. Here, we consider a thin lens for calculation because of the small size of the laser beam operating in the paraxial region.

We attain the value of s_2 by substitution of s_1 from (1):

$$s_2 = \frac{f_1(2\Delta - f_1)}{2\Delta} - l \tag{4}$$

As lens L_2 is technically an array of microlens, the location of each lens can be denoted as a coordinate in a m × n matrix (see Figure 3). The optical center ρ_{mn} of each lens can be determined by using polar coordinates:

$$\rho_{mn} = p \times \sqrt{\left(\frac{M+1}{2} - m\right)^2 + \left(\frac{N+1}{2} - n\right)^2} \tag{5}$$

$$\tan\varphi = \frac{\left|\frac{M+1}{2} - m\right|}{\left|\frac{N+1}{2} - n\right|} \tag{6}$$

Here, ρ_{mn} is the position of the optical center of microlens at row m, column n, p is the microlens step, φ is the angular coordinate, M and N are the number of rows and columns respectively on the lens array (as in Figure 3, $M = N = 9$). Laser beam diameter d_2 ensures a smaller size than lens L_2 calculated according to the relationship:

$$d_2 = -2.s_2.\tan\beta \tag{7}$$

Besides, the ratio relationship:

$$\frac{\tan\beta}{\tan\alpha} = \frac{s_1}{l + s_2} = \frac{2\Delta - f_1}{l + \left[\frac{f_1(2\Delta - f_1)}{2\Delta} - l\right]} = \frac{2\Delta}{f_1} \tag{8}$$

Substituting (2) into (8) we can calculate:

$$\tan\beta = \frac{2\Delta}{f_1} \cdot \frac{d}{2f_1} = \frac{d\Delta}{f_1^2} \tag{9}$$

Knowing s_2, $tan\beta$ and the distance deviation from the focus point Δ, we can calculate d_2, from which we have a reasonable size of the L_2 microlens, ensuring the laser spot lies completely on the L_2.

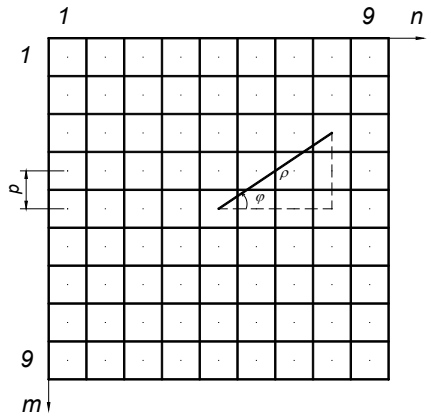

Figure 3
Microlens array size m×n

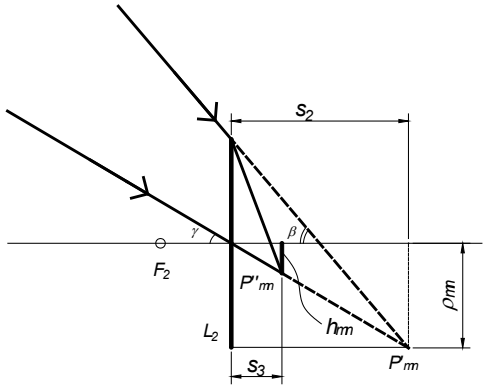

Figure 4
Schematic of optical path on a microlens

Apply the same procedure of calculation at lens L_1 to lens L_2:

$$s_3 = \frac{s_2 . f_2}{s_2 + f_2} \tag{10}$$

The collimated laser beam reaches L_2 with $\beta = 0$ is split into $M \times N$ spots on IS, with distance between each two spots $P''_{\beta=0} = p$. Consider any incident laser beam with $\beta \neq 0$ to lens L_2, the spot positions on IS will have a displacement of h_{mn} from point $P''_{\beta=0}$ (see Figure 4):

$$h_{mn} = \frac{s_3}{s_2} \rho_{mn} = \frac{f_2}{s_2 + f_2} \rho_{mn} \tag{11}$$

At $\rho_{mn} = 0$, which is right at the center of microlens, image created by this lens at this specific position is always fixed, while the further the microlens from the center, the greater the displacement of its created image. As f_2 increases, the displacement hmn increases, follows by the improvement in resolution for Δ detection.

Substitute equation (11) to (4), we attained Δ:

$$\Delta = \frac{f_1^2}{2.\left(f_1 + f_2 - l - \frac{\rho_{mn}}{h_{mn}} f_2\right)} \tag{12}$$

By calculating the distance hmn on the $(m \times n)^{th}$ microlens at the IS, we can determine the defocus length Δ from (12).

To solve the impact of optical aberrations to the spots position we know that only spherical aberration which are directly related to wavefront error after goes through objective lens two times including incident and reflection at sample surface. Due to laser source is always parallel to the optical axis and the reflection point is on the optical axis, the objective lens has no off-axis aberration. Referring first problem above, the aberrated wavefront affects to spots position so we use wave aberration expression to describe the affection (Eq. (13))

$$W(H, \rho, \theta) = W_{040}^{(1)} - W_{040}^{(2)} \tag{13}$$

Where W – wave aberration function; $W_{040}^{(1)}$, $W_{040}^{(2)}$ – spherical aberration coefficients for two times passing L_1; H – normalized object height or angle; ρ and θ – normalized polar coordinates at exit pupil.

As the aberration theory, the variation of point on image plane will be calculated based on differential wave aberration function. Finally, we get the displacements following x- and y-axis at the image plane:

$$\begin{cases} \varepsilon_x = -\frac{4R}{n' r_P} W_{040} x_P^3 \\ \varepsilon_y = -\frac{4R}{n' r_P} W_{040} y_P^3 \end{cases} \tag{14}$$

Where ε_x, ε_y - displacement from paraxial image; R – reference sphere radius (equal to focal length of L1); n' – environment refractive index (n'=1); r_p – radius of exit pupil ($s_2 tan\beta$); x_p, y_p – normalized coordinates an exit pupil. W_{040} is expressed in Seidel aberration $W_{040} = \frac{1}{8} S_I$ with

$$S_I = -\sum A^2 y \Delta\left\{\frac{u}{n}\right\} \tag{15}$$

Where:

$$A = n(u + yC)$$

Knowing refractive index of L_1 (n), marginal ray angle and height u, y, curvature (C) we can calculate spherical aberration for the image by applying equation (14).

Because of axial symmetry, the spots move to center by ε:

$$\varepsilon = \sqrt{\varepsilon_x^2 + \varepsilon_y^2} = \frac{4R}{n' r_P} W_{040} \sqrt{x_P^6 + y_P^6} \tag{16}$$

Or calculated by microlens array polar coordinate $x_p = \rho\cos\varphi$ and $y_p = \rho\sin\varphi$:

$$\varepsilon = \sqrt{\varepsilon_x^2 + \varepsilon_y^2} = \frac{4R}{n' r_P} W_{040} \rho^3 \sqrt{\cos^6\varphi + \sin^6\varphi} \tag{17}$$

3 Results and Discussions

To verify the theoretical model above, we perform simulations on OpticStudio (Figure 5). The laser source used in the process has a wavelength of 635 nm, with beam divergence of 0.6 mrad. The microlens array (L_2) is a square grid of size 15×15 mm, and has focal distance f_2 =12.621 mm, with lenslet pitch 300 μm. For more details of input parameters, refer to Table 1.

Table 1
Parameters applied in simulation process

Laser source	λ = 635 nm d = 3.0 mm Beam divergence: 0.6 mrad
Objective lens (L_1)	Material: N-BK7 Refractive index: 1.515 f_1 = 15.075 mm t = 3 mm Diameter: 10 mm
Microlens array (L_2)	Material: N-BK7 Refractive index: 1.515 Focal distance f_2: 12.621 mm Lenslet pitch (p): 300 μm Array size: 15×15 mm, square grid
Distances	l_1 = 30 mm (L_1 to BS) l_2 = 20 mm (L_2 to BS)

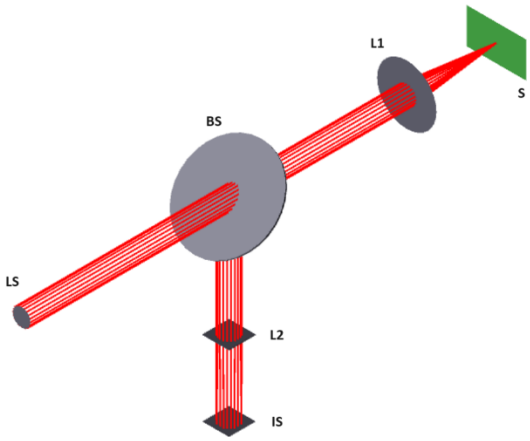

Figure 5
Schematic of the simulated optical system for focal point detection on OpticStudio. LS-Laser source; BS-Beam splitter; L1-Objective lens; L2-Microlens array; IS-Image sensor; S-Sample surface.

Consider the position where the target surface lies on the focal plane of L_1, the incident beam goes through microlens array L_2, results in several focal points, distancing 0.3 mm from each other (Figure 6-c,d). Displace the surface toward L_1 ($\Delta > 0$), the beam to L_2 diverges, resulting in beam diameter greater than d, the laser beam converges at distance $0.3+h_{mn}$ away from L_2 (Figure 6-a,b). Similarly, with $\Delta < 0$, the laser beam converges at distance $0.3-h_{mn}$ (Figure 6-e,f).

With parameters f_1 = 15.075 mm, f_2 = 12.621 mm, $l = l_1 + l_2$ = 50.00 mm, Eq. (12) gives Δ is:

$$\Delta = \frac{227.256}{-44.608 - 25.242.\Gamma} \tag{18}$$

with $\Gamma = \frac{\rho_{mn}}{h_{mn}}$ is the ratio of magnification.

Firstly, we adjust the sample to focal plane of L_1 (position 1) and capture this image; then we move the sample toward the L_1 0.1 mm (position 2) and capture it again. So, we have two images with the intensity distribution on IS. The points displacement between theses position are h in Table 2.

With M=N=15, Δ = 0.1 mm, we find s_2=-1171.203 mm, d_2 = 3.092 mm so ρ_{max} = 1.454 mm (the spot cover matrix lenslet from (3,3) to (13,13)). Due to blur of laser spot, so the effective area from (4,4) to (12,12) on the microlens array was chosen (Table 2 and Table 3).

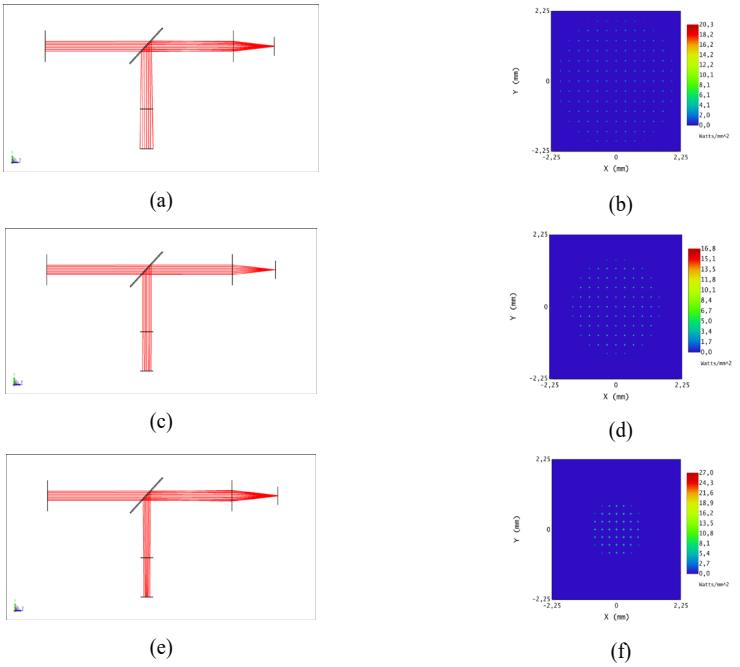

Figure 6
Simulation results at different position of the sample surface
(a), (b) Front-focus, (c), (d) In-focus, (e), (f) Back-focus

Table 2
Center of the spot coordinates at position 1 (Unit: mm)

(-1.180, -1.180)	(-0.896, -1.193)	(-0.601, -1.200)	(-0.301, -1.204)	(0.000, -1.206)	(0.301, -1.204)	(0.601, -1.200)	(-0.896, -1.193)	(1.180, -1.180)
(-1.193, -0.896)	(-0.902, -0.902)	(-0.605, -0.907)	(-0.303, -0.910)	(0.000, -0.910)	(0.303, -0.910)	(0.605, -0.907)	(-0.902, -0.902)	(1.193, -0.896)
(-1.200, -0.601)	(-0.907, -0.605)	(-0.607, -0.607)	(-0.304, -0.609)	(0.000, -0.611)	(0.304, -0.609)	(0.607, -0.607)	(-0.907, -0.605)	(1.200, -0.601)
(-1.204, -0.301)	(-0.910, -0.303)	(-0.609, -0.304)	(-0.305, -0.305)	(0.000, -0.306)	(0.305, -0.305)	(0.609, -0.304)	(-0.910, -0.303)	(1.204, -0.301)
(-1.206, -0.000)	(-0.910, -0.000)	(-0.611, -0.000)	(-0.306, -0.000)	(0.000, -0.000)	(0.306, -0.000)	(0.611, -0.000)	(-0.910, -0.000)	(1.206, -0.000)
(-1.204, 0.301)	(-0.910, 0.303)	(-0.609, 0.304)	(-0.305, 0.305)	(0.000, 0.306)	(0.305, 0.305)	(0.609, 0.304)	(-0.910, 0.303)	(1.204, 0.301)
(-1.200, 0.601)	(-0.907, 0.605)	(-0.607, 0.607)	(-0.304, 0.609)	(0.000, 0.611)	(0.304, 0.609)	(0.607, 0.607)	(-0.907, 0.605)	(1.200, 0.601)
(-1.193, 0.896)	(-0.902, 0.902)	(-0.605, 0.907)	(-0.303, 0.910)	(0.000, 0.910)	(0.303, 0.910)	(0.605, 0.907)	(-0.902, 0.902)	(1.193, 0.896)
(-1.180, 1.180)	(-0.896, 1.193)	(-0.601, 1.200)	(-0.301, 1.204)	(0.000, 1.206)	(0.301, 1.204)	(0.601, 1.200)	(-0.896, 1.193)	(1.180, 1.180)

Table 3
Center of the spot coordinates at position 2 (Unit: mm)

(-1.197, -1.197)	(-0.907, -1.210)	(-0.607, -1.216)	(-0.305, -1.219)	(0.000, -1.220)	(0.305, -1.219)	(0.607, -1.216)	(0.907, -1.210)	(1.197, -1.197)
(-1.210, -0.907)	(-0.914, -0.914)	(-0.612, -0.917)	(-0.307, -0.920)	(0.000, -0.921)	(0.307, -0.920)	(0.612, -0.917)	(0.914, -0.914)	(1.210, -0.907)
(-1.216, -0.607)	(-0.917, -0.612)	(-0.614, -0.614)	(-0.308, -0.615)	(0.000, -0.616)	(0.308, -0.615)	(0.614, -0.614)	(0.917, -0.612)	(1.216, -0.607)
(-1.219, -0.305)	(-0.920, -0.307)	(-0.615, -0.308)	(-0.308, -0.308)	(0.000, -0.308)	(0.308, -0.308)	(0.615, -0.308)	(0.920, -0.307)	(1.219, -0.305)
(-1.220, -0.000)	(-0.921, -0.000)	(-0.616, -0.000)	(-0.308, -0.000)	(0.000, -0.000)	(0.308, -0.000)	(0.616, -0.000)	(0.921, -0.000)	(1.220, -0.000)
(-1.219, 0.305)	(-0.920, 0.307)	(-0.615, 0.308)	(-0.308, 0.308)	(0.000, 0.308)	(0.308, 0.308)	(0.615, 0.308)	(0.920, 0.307)	(1.219, 0.305)
(-1.216, 0.607)	(-0.917, 0.612)	(-0.614, 0.614)	(-0.308, 0.615)	(0.000, 0.616)	(0.308, 0.615)	(0.614, 0.614)	(0.917, 0.612)	(1.216, 0.607)
(-1.210, 0.907)	(-0.914, 0.914)	(-0.612, 0.917)	(-0.307, 0.920)	(0.000, 0.921)	(0.307, 0.920)	(0.612, 0.917)	(0.914, 0.914)	(1.210, 0.907)
(-1.197, 1.197)	(-0.907, 1.210)	(-0.607, 1.216)	(-0.305, 1.219)	(0.000, 1.220)	(0.305, 1.219)	(0.607, 1.216)	(0.907, 1.210)	(1.197, 1.197)

Next, we calculate the spherical aberration for L_1 using equation (14) and (15) with notation as show in Figure 7.

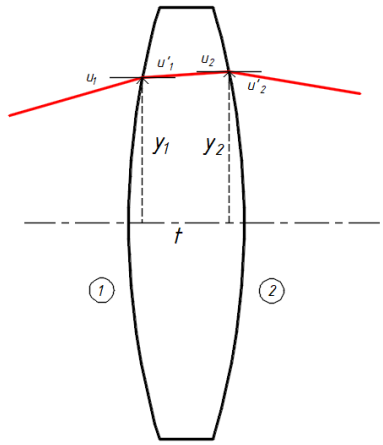

Figure 7
Diagram for optical aberration calculations

Incident (path 01):

	Surface ①		Surface ②	
	n = 1	n' = 1.515	n = 1.515	n' = 1
C (mm^{-1})	0.067		-0.067	
y (mm)	1.5		1.399	
u (rad)	0	-0.034	-0.034	-0.099
A	0.1		-0.194	

S_I	-0.00034	-0.004
$W_{040}^{(1)}$ (mm)	0.0005425	

Reflection (path 02):

	Surface ②		Surface ①	
	n = 1	n' = 1.515	n = 1.515	n' = 1
C (mm^{-1})	0.067		-0.067	
y (mm)	1.480		1.577	
u (rad)	0.099	0.032	0.032	-0.005
A	0.198		-0.111	
S_I	-0.005		-0.001	
$W_{040}^{(2)}$ (mm)	0.001			

By substituting value $W_{040}^{(1)}$ and $W_{040}^{(2)}$ in equation (13), (17) we attained ε:

$$\varepsilon = \frac{4 \times 15.075}{1 \times 1.546}(0.0005425 - 0.001)\rho^3\sqrt{\cos^6\varphi + \sin^6\varphi}$$

$$\varepsilon = -0.018\rho^3\sqrt{\cos^6\varphi + \sin^6\varphi}$$

Table 4

Spherical aberration value ε for Δ = 0.1 mm

-0.044	-0.033	-0.031	-0.031	-0.031	-0.031	-0.031	-0.033	-0.044
-0.033	-0.018	-0.014	-0.013	-0.013	-0.013	-0.014	-0.018	-0.033
-0.031	-0.014	-0.005	-0.004	-0.004	-0.004	-0.005	-0.014	-0.031
-0.031	-0.013	-0.004	-0.001	0.000	-0.001	-0.004	-0.013	-0.031
-0.031	-0.013	-0.004	0.000	0.000	0.000	-0.004	-0.013	-0.031
-0.031	-0.013	-0.004	-0.001	0.000	-0.001	-0.004	-0.013	-0.031
-0.031	-0.014	-0.005	-0.004	-0.004	-0.004	-0.005	-0.014	-0.031
-0.033	-0.018	-0.014	-0.013	-0.013	-0.013	-0.014	-0.018	-0.033
-0.044	-0.033	-0.031	-0.031	-0.031	-0.031	-0.031	-0.033	-0.044

Similar calculations, we get the ε for Δ = 0:

Table 5

Spherical aberration value ε for Δ = 0 mm

-0.045	-0.034	-0.032	-0.032	-0.032	-0.032	-0.032	-0.034	-0.045
-0.034	-0.019	-0.014	-0.013	-0.013	-0.013	-0.014	-0.019	-0.034
-0.032	-0.014	-0.006	-0.004	-0.004	-0.004	-0.006	-0.014	-0.032
-0.032	-0.013	-0.004	-0.001	0.000	-0.001	-0.004	-0.013	-0.032
-0.032	-0.013	-0.004	0.000	0.000	0.000	-0.004	-0.013	-0.032
-0.032	-0.013	-0.004	-0.001	0.000	-0.001	-0.004	-0.013	-0.032
-0.032	-0.014	-0.006	-0.004	-0.004	-0.004	-0.006	-0.014	-0.032

-0.034	-0.019	-0.014	-0.013	-0.013	-0.013	-0.014	-0.019	-0.034
-0.045	-0.034	-0.032	-0.032	-0.032	-0.032	-0.032	-0.034	-0.045

Using ε to eliminate spherical aberration of two images at position 1 and 2 then using linear fitting to find the function $h=f(\rho)$:

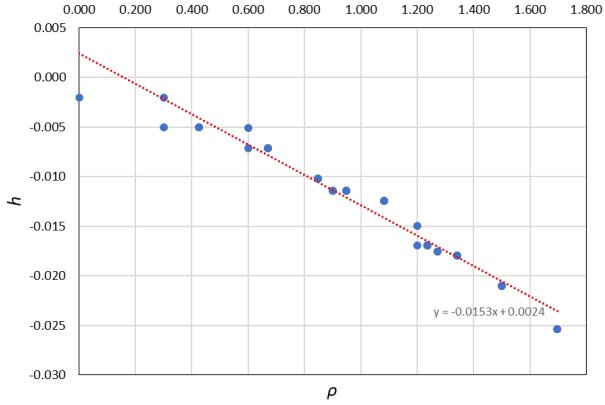

Figure 8
Relationship between the h and ρ

$$h= -0.0153\rho+0.0024 \quad (19)$$

To verify the result, we pick any ρ, here ρ = 0.671 (microlens locates at (8,6)), we evaluate the value Δ = -0.108 with a different of 8% to the simulation.

Conclusion

The proposed method and simulation in OpticStudio allow rapid detection for laser auto-focusing system. The results show a reliable detection method, with high accuracy measurement in both directions and distances from the target surface. Through this simulation, we can evaluate the model before applying it on laboratory experiments with optical components, with a difference of 8% to the theoretical calculation. This system is proven with high sensitivity to the deviation of the laser beam on the sample surface. This method is feasible and can be dedicated to applying in real-time laser manufacturing with high precision.

Acknowledgement

This work was funded by the Vietnam Ministry of Education and Training under Project Number B2024-BKA-12.

References

[1] S. Cai, Y. Sun, H. Chu, W. Yang, H. Yu, and L. Liu, “Microlenses arrays: Fabrication, materials, and applications,” Microsc Res Tech, Vol. 84, No. 11, pp. 2784-2806, Nov. 2021, doi: 10.1002/JEMT.23818

[2] J. Chen, M. Chen, H. Wu, S. Xie, and T. Kiyoshi, "Distortion spot correction and center location base on deep neural network and MBAS in measuring large curvature aspheric optical element," Opt Express, Vol. 30, No. 17, p. 30466, Aug. 2022, doi: 10.1364/OE.462482

[3] Z. Ge, Z. Liu, Y. Huang, Y. Huang, and Z. Lv, "Analysis and design of a microlens array scanning system based on spherical aberration," Applied Optics, Vol. 62, Issue 1, pp. 227-234, Vol. 62, No. 1, pp. 227-234, Jan. 2023, doi: 10.1364/AO.468180

[4] Y. J. Chang, C. Y. Wang, J. C. Hsu, C. C. Ho, and C. L. Kuo, "Real-time laser-induced plasma monitoring in percussion pulsed laser material processing," Measurement, Vol. 135, pp. 905-912, Mar. 2019, doi: 10.1016/J.MEASUREMENT.2018.12.042

[5] C. C. Ho and J. J. He, "On-line monitoring of laser-drilling process based on coaxial machine vision," International Journal of Precision Engineering and Manufacturing, Vol. 15, No. 4, pp. 671-678, Apr. 2014, doi: 10.1007/S12541-014-0386-X/METRICS

[6] C. C. Ho, Y. J. Chang, J. C. Hsu, C. M. Chiu, and C. L. Kuo, "Optical emission monitoring for defocusing laser percussion drilling," Measurement, Vol. 80, pp. 251-258, Feb. 2016, doi: 10.1016/J.MEASUREMENT.2015.10.031

[7] B. X. Cao, P. Le Hoang, S. Ahn, J. o. Kim, H. Kang, and J. Noh, "Real-time laser focusing system for high-precision micromachining using diffractive beam sampler and advanced image sensor," Opt Lasers Eng, Vol. 107, pp. 13-20, Aug. 2018, doi: 10.1016/J.OPTLASENG.2018.03.002

[8] S. Ahn, B. X. Cao, P. H. Le, H. Kang, J. Kim, and J. Noh, "Automatic real-time focus control system for laser processing using dynamic focusing optical system," Optics Express, Vol. 25, Issue 23, pp. 28427-28441, Vol. 25, No. 23, pp. 28427-28441, Nov. 2017, doi: 10.1364/OE.25.028427

[9] A. Kacaras, M. Bächle, M. Schwabe, F. Zanger, F. P. León, and V. Schulze, "Acoustic emission-based characterization of focal position during ultra-short pulse laser ablation," Procedia CIRP, Vol. 81, pp. 270-275, Jan. 2019, doi: 10.1016/J.PROCIR.2019.03.047

[10] Y. Cai and N. H. Cheung, "Photoacoustic monitoring of the mass removed in pulsed laser ablation," Microchemical Journal, Vol. 97, No. 2, pp. 109-112, Mar. 2011, doi: 10.1016/J.MICROC.2010.08.001

[11] B. X. Cao, P. Le Hoang, S. Ahn, J. O. Kim, H. Kang, and J. Noh, "In-Situ Real-Time Focus Detection during Laser Processing Using Double-Hole Masks and Advanced Image Sensor Software," Sensors 2017, Vol. 17, p. 1540, Vol. 17, No. 7, p. 1540, Jul. 2017, doi: 10.3390/S17071540

[12] B. Xuan Cao, P. Le Hoang, S. Ahn, J. o. Kim, H. Kang, and J. Noh, "Measurement of focal length based on laser-beam-spot tracking system

using diffractive beam sampler," Measurement (Lond), Vol. 122, pp. 135-140, Jul. 2018, doi: 10.1016/j.measurement.2018.03.011

[13] B. X. Cao et al., "Design and Performance of a Focus-Detection System for Use in Laser Micromachining," Micromachines 2016, Vol. 7, p. 2, Vol. 7, No. 1, p. 2, Jan. 2016, doi: 10.3390/MI7010002

[14] M. Chen, S. Takahashi, and K. Takamasu, "Multi-beam angle sensor for flatness measurement of mirror using circumferential scan technology," International Journal of Precision Engineering and Manufacturing, Vol. 17, No. 9, pp. 1093-1099, Sep. 2016, doi: 10.1007/S12541-016-0133-6/METRICS

[15] M. Chen, S. Takahashi, and K. Takamasu, "Development of high-precision micro-roundness measuring machine using a high-sensitivity and compact multi-beam angle sensor," Precis Eng, Vol. 42, pp. 276-282, Oct. 2015, doi: 10.1016/J.PRECISIONENG.2015.05.009

[16] Warren J. Smith, Modern optical engineering, Third edition. New York: McGraw-Hill, 2000